Int. J. Electrochem. Sci., 15 **(2020)** 12690 – 12705, doi: 10.20964/2020.12.36

International Journal of
ELECTROCHEMICAL
SCIENCE
www.electrochemsci.org

Investigation of 1,1-didecyl-4,4-bipyridine and 1,1-didecyl-2,2-bipyridine as Corrosion Inhibitors for Carbon Steel in Hydrochloride Acid Solution

Xian He[1], Lu Chen[1], Yang Tian[1], Fubin Ma[2], Xi Huang[1,3], Kun Cao[1,]*

[1] Department of Chemistry & Chemical Engineering, Neijiang Normal University, Neijiang, Sichuan, 641112, PR China
[2] Institute of Oceanology, Chinese Academy of Sciences, Qingdao, 266000, China
[3] Material Corrosion and Protection Key Laboratory of Sichuan province, Sichuan University of Science and Engineering, Zigong, Sichuan, 643000, PR China
[*]E-mail: kevin_cao0811@126.com

Received: 19 July 2020 / *Accepted:* 22 September 2020 / *Published:* 31 October 2020

Bipyridine surfactants (BPSs) were analyzed as corrosion inhibitors for mild steel in 1 mol·L^{-1} HCl. The corrosion behavior was evaluated using weight loss method, potentiodynamic polarization, and electrochemical impedance spectroscopy. The results show that the anticorrosive efficiency increased with increasing concentration of BPSs. In addition, BPSs behaved as a mixed-type inhibitor based on the anode. The surface of steel was examined by scanning electron microscopy, atomic force microscopy, and X-ray phosphorescence spectroscopy. The elemental analysis of the chemical states on the surface indicated that BPSs adsorbed on mild steel surface to prevent corrosion.

Keywords: mild steel; corrosion inhibitor; bipyridine; electrochemical

1. INTRODUCTION

Metal corrosion is caused by the electrochemical and chemical interaction between the metal surface and the surrounding environment, causing gradual destruction of metal structure integrity [1]. Since metal corrosion cannot be evitable, prevention and mitigation of corrosion are a common strategy in industry. Among the anti-corrosion methods, the use of corrosion inhibitors is a common and important method [2]. Different types of organic compounds, containing N, S, O, and π-electrons have high potential to be applied as inhibitors to prevent corrosion [3–8]. Many synthetic organic compounds have been proven to be effective corrosion inhibitors for slowing down the corrosion; however many new and efficient corrosion inhibitor have not been widely used because of their harmful effect on human

and environment [9]. Therefore, developing eco-friendly corrosion inhibitors instead of highly toxic ones has become a new area of interest [10–12].

Surfactants have been extensively used as corrosion inhibitors in different media. Espinosa *et al.* [13] studied four types of imidazolium surfactants with long alkyl chain as corrosion inhibitors for copper in air, indicating that the inhibitors could react with copper to form the corresponding copper sulfate salt, increasing the roughness and hydrophobicity of the copper surface. Kowsari *et al.* [14] found that surfactants with amino functional group have good anti-corrosion performance for mild steel in 1 mol/L HCl solution, and such inhibitors decreased the corrosion rate by inhibiting anodic dissolution. Tawfik *et al*. [15] synthesized three gemini surfactants as corrosion inhibitors, where the inhibitors could adsorb on mild steel surface to form a monomolecular layer, following the Langmuir adsorption isotherm model.

This study aimed to investigate the inhibition efficiency of two bipyridine surfactants (BPSs) on mild steel in 1 $mol \cdot L^{-1}$ HCl solutions. The anti-corrosion performances were examined by electrochemical measures and weight loss test. The interaction between the active component and the surface of mild steel were characterized *via* X-ray photoelectron spectroscopy (XPS). The surface characteristics of mild steel were investigated in detail by scanning electron microscopy (SEM) and atomic force microscopy (AFM). Finally, the possible inhibition mechanisms of the BPSs were proposed by Langmuir adsorption isotherm.

2. EXPERIMENTAL

2.1 Materials and chemicals

Bipyridine surfactants named 1,1-didecyl-4,4-bipyridine (4-BP) and 1,1-didecyl-2,2-bipyridine (2-BP) shown in Fig. 1 were synthesized according to the following procedures. Briefly, 0.2 mol 4,4-bipyridine/ 2,2-bipyridine was dissolved in acetonitrile, and the resulting solution was stirred under heating at 100 °C in N_2 atmosphere, followed by dropwise addition of 0.4 mol bromodecane to the mixture solution and reacted further for 40 h. The acetonitrile in the reaction mixture was removed by rotary evaporation. The products were washed with ethyl ether and vacuum dried. The structures of the two pure BPSs were characterized by FTIR in the frequency range 4000–400 cm^{-1}.

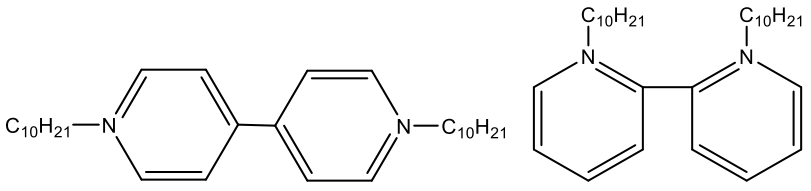

Figure 1. The structure of 4-BP and 2-BP

2.2 Preparation of corrosive medium and mild steel specimens

The corrosive medium (1 mol·L^{-1} HCl) was prepared by diluting HCl (37%) with distilled water and used as the control sample. BPSs in the concentration range 1×10^{-5}–1×10^{-2} mol/L were added to the 1 mol·L^{-1} HCl solution. Mild steel (Q235) was used as the working electrode. The specimens used in all the experiments were manually abraded using SiC paper with the grit size of 400 and 1000 and treated with α-Al_2O_3 polishing powder (0.3 μm), washed sequentially with distilled water, ethanol, and acetone, and then dried at room temperature.

2.3 Weight Loss Measurements

The weight loss test was performed in the corrosive medium with different concentrations of BPSs according the rule of the ASTM G1-03. The average weight loss of mild steel samples was expressed by the corrosion rate (CR), and corrosion inhibition efficiency (η) was calculated by the following equations, where Δw is the mean weight loss, d is the density of mild steel, A is the average surface area of the specimen, and t is the immersion time. In this study, the average surface area of the specimen is approximately 23 cm^2, the density of mild steel is 7.85 g·cm^{-3}, and the immersion time is 3 h at different temperatures (298, 308, and 318 K).

$$CR(mm\ per\ year) = \frac{87600\times\Delta w(g)}{d(g\cdot cm^{-3})\times A(cm^2)\times t(h)} \quad (1)$$

$$\eta(\%) = \frac{CR - CR_{inh}}{CR}\times 100 \quad (2)$$

2.4 Electrochemical Measurements

The electrochemical measurements were performed using an Ivium electrochemical workstation. A three-electrode system was used: mild steel (1 cm^2) as the working electrode, platinum as the counter electrode, and Ag|AgCl as the reference electrode. The three electrodes were immersed in the test solution for 0.5 h before the electrochemical test to stabilize the system.

Electrochemical impedance spectroscopy (EIS) was performed with an amplitude of 10 mV and in the range from 100 kHz to 10 mHz in potentiostatic mode at the OCP. Then, polarization curves were obtained at a scan rate of 1 mV·s^{-1}.

The efficiency of BPSs was calculated from the electrochemical test by Eqs. 3 and 4.

$$\eta_R(\%) = \frac{R_{ct} - R_{ct}^0}{R_{ct}}\times 100 \quad (3)$$

$$\eta_i(\%) = \frac{i_{corr}^0 - i_{corr}}{i_{corr}^0}\times 100 \quad (4)$$

where R_{ct} is the charge transfer resistance with the inhibitor and R^0_{ct} is the charge transfer resistance without inhibitor, i^0_{corr} and i_{corr} are the corrosion current densities with and without inhibitor, respectively.

2.5 Surface analysis

All specimens used for surface analysis were removed from the corrosive solutions in the presence and absence of BPSs after 3 h immersion, and their surfaces were vigorously washed using distilled water and dried under vacuum before use.

The morphologies of the mild steel were determined using a TEDCAN VEGA 3 SBH model scanning electron microscope and a Bruker MULTIMODE 8 atomic force microscope under ambient conditions. AFM images were obtained in the tapping mode at a scan rate of 2.5 Hz. The XPS measurement was performed using a PHI5000-VersaProbe system, with Mg Kα radiation as the excitation source.

3. RESULTS AND DISCUSSION

3.1 FTIR analysis

To identify the major groups of the BPSs. The FTIR peaks of 4-BP are as follows: 3100 cm^{-1}, 3000 cm^{-1} [*v* (Ar-H)], 2915 cm^{-1}, 2850 cm^{-1} [*v* (C-H)], 1957 cm^{-1} (the vibration of conjugated π bond within the pyridine ring), 1635 cm^{-1} [*v* (C=N)], 1556 cm^{-1}, 1467 cm^{-1} [*v* (C=C)], 1176 cm^{-1} [*v* (C–C)]; 719 cm^{-1} [(CH_2)n, n >4]; for 2-BP: 3106 cm^{-1}, 3004 cm^{-1} [*v* (Ar–H)], 2915 cm^{-1}, 2848 cm^{-1} [*v* (C–H)]; 1951 cm^{-1} (the vibration of conjugated π bond within the pyridine ring), 1637 cm^{-1} [*v* (C=N)], 1557 cm^{-1}, 1466 cm^{-1} [*v* (C=C)], 1176 cm^{-1} [*v* (C–C)]; 719 cm^{-1} [(CH_2)n, n >4].

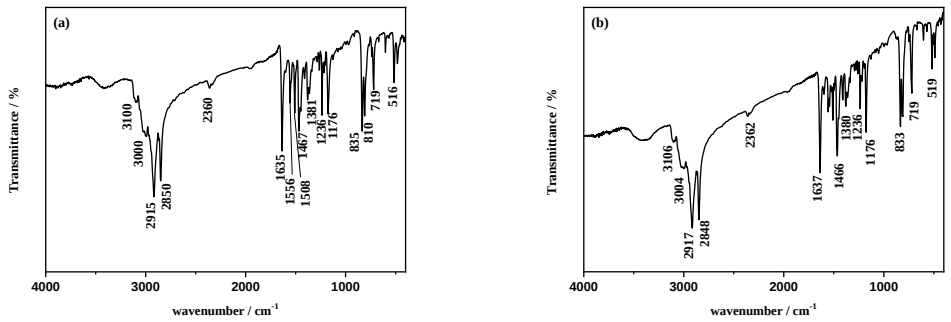

Figure 2. FTIR analysis of 4-BP (a) and 2-BP (b)

3.2Weight loss test

Table 1. Weight loss data of the carbon steel with inhibitors in 1mol/L HCl at different temperature.

Inhibitor	C (mol·L^{-1})	298K			308K			318K		
		Δw (mg)	CR (mmpy)	η (%)	Δw (mg)	CR (mmpy)	η (%)	Δw (mg)	CR (mmpy)	η_{ew} (%)
Blank	0	62.4	8.34	--	64.9	8.68	--	66.3	8.86	--
4-BP	1×10^{-5}	13.5	1.81	78.4	17.2	2.30	76.5	20.9	2.79	72.8
	1×10^{-4}	10.2	1.36	83.7	12.8	1.71	80.3	15.0	2.01	77.4
	1×10^{-3}	6.34	0.848	89.8	10.1	1.35	84.4	13.1	1.75	80.3
	1×10^{-2}	4.13	0.552	93.4	7.45	0.996	88.1	9.18	1.23	85.7
2-BP	1×10^{-5}	14.1	1.89	77.4	18.5	2.47	70.4	21.2	2.83	68.0
	1×10^{-4}	10.8	1.44	82.7	14.3	1.91	77.1	17.6	2.35	73.5
	1×10^{-3}	7.59	1.02	87.8	11.2	1.50	82.1	14.2	1.90	78.6
	1×10^{-2}	5.23	0.699	91.6	8.52	1.14	86.4	13.5	1.81	84.6

Table 1 shows the dependence of inhibition efficiency (η) on varying concentrations of BPSs in the range 1×10^{-5}–1×10^{-2} mol/L. BPSs displayed good inhibition efficiency. The inhibition efficiency increased with increasing concentration of BPSs, giving a maximum at 1×10^{-2} mol/L and, and a small change in inhibition efficiency was observed with varying temperature from 298 K to 318 K.

3.3 Impedance measurements

Electrochemical impedance spectroscopy was carried out to establish the adsorption and inhibition mechanism of BPSs on the mild steel/solution interface. Fig. 3 shows the Nyquist plots for mild steel at open-circuit potential after an exposure of 0.5 h in 1 mol·L^{-1} HCl solution at 298 K. The Nyquist plots show a depressed capacitive loop, which can be attributed to the charge transfer reaction and time constant of the electric double layer and to the surface inhomogeneity of structural or interfacial origin, such as those found in adsorption processes [16,17]. Moreover, these diagrams have a similar shape, which is maintained throughout all the tested concentrations, indicating that almost no change in the corrosion mechanism occurs as a result of the inhibitor addition. Furthermore, the diameter of the shape increased after the addition of organic compounds to the corrosive solution. This increase was more and more pronounced with increasing inhibitor concentration, indicating that the adsorption of inhibitor molecules on the metal surface inhibited the dissolution of mild steel [18–20].

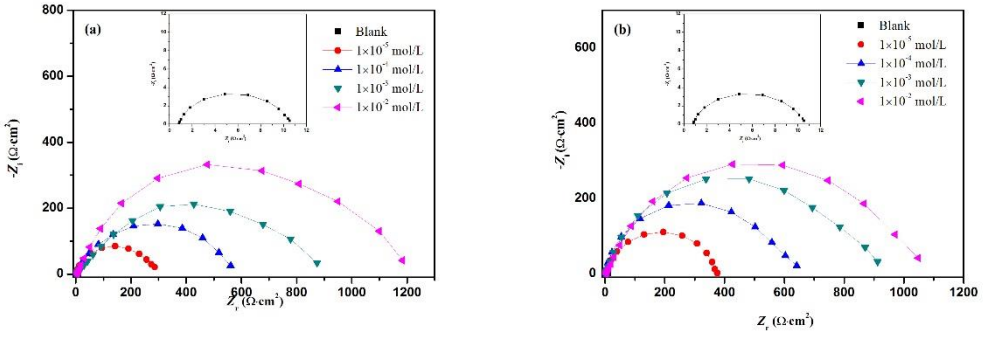

Figure 3. Nyquist plots of mild steel in 1 mol/L HCl solution with different concentrations of 4-BP (a) and 2-BP (b)

The impedance spectra for the Nyquist plots were analyzed by fitting to the equivalent circuit model (Fig. 4), describe elsewhere for iron/acid interface.

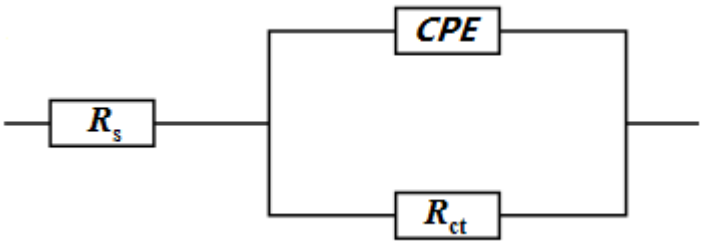

Figure 4. Equivalent circuit for impedance analysis

In Fig. 4, R_s is the solution resistance, R_{ct} is the charge transfer resistance and CPE is the constant phase element. The impedance of the CPE is expressed as follows:

$$Z_{CPE} = \frac{1}{Y_0 (j\omega)^n} \quad (5)$$

where Y_0 is the CPE constant, n is the CPE exponent, which can be used as a gauge of the topoghraphical heterogeneity or roughness of the surface, $j^2 = -1$ is an imaginary number, and ω is the angular frequency in rad s^{-1}. Depending on the value of n, CPE can represent a resistance (Z_{CPE} = R, n = 0); a capacitance (Z_{CPE} = C, n = 1), a Warburg impedance (Z_{CPE} = W, n = 0.5) or an inductance (Z_{CPE} = L, n = -1) [21].

The impedance parameters for mild steel in 1 mol·L^{-1} HCl solution at 298 K are listed in Table 2.

Table 2. EIS parameters of mild steel in 1 mol·L^{-1} HCl containing various concentrations of BPSs

Inhibitors	C (mol·L^{-1})	R_s (Ω·cm^2)	CPE		R_{ct} (Ω·cm^2)	η_R (%)
			Y_0 (μF·cm^{-2})	n		
Blank	0	0.7485	446	0.79	9.888	—
4-BP	1×10^{-5}	1.625	150.9	0.78	273.4	96.4
	1×10^{-4}	1.435	134.6	0.75	584.9	98.3
	1×10^{-3}	1.483	122.9	0.76	885.7	98.9
	1×10^{-2}	1.525	112.2	0.78	1182	99.2
2-BP	1×10^{-5}	1.059	397.5	0.73	378.1	97.4
	1×10^{-4}	1.771	320.4	0.76	638.4	98.5
	1×10^{-3}	1.991	217.5	0.75	912.9	98.9
	1×10^{-2}	1.393	140.7	0.75	1022	99.0

The data in Table 2 indicate that the R_{ct} increased with increasing concentration of BPSs, whereas the values of Y_0 decreased by increasing inhibitor concentrations, suggesting that the amount of inhibitor molecules adsorbed on the electrode surface gradually increased and replaced the water molecules at the film/solution interface, consequently decreasing the active sites necessary for the coupled dissolution reaction. The maximum values of η_R reached 99.2% and 99.0% for 4-BP and 2-BP, respectively.

3.4 Polarization curve measurements

Potentiodynamic polarization curves for mild steel in 1 mol/L HCl solution in the absence and presence of various concentrations of BPSs at 298 K are shown in Fig. 5.

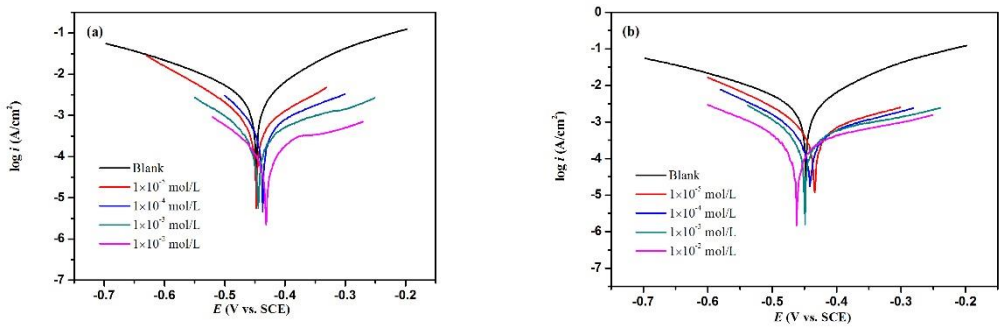

Figure 5. Polarization curves for the mild steel in 1 mol·L^{-1} HCl solution containing various concentrations of 4-BP (a) and 2-BP (b)

The presence of inhibitors lowers the corrosion current density largely for the anodic branch than for the cathodic lines, thereby indicating the greater suppression of the anodic dissolution of Fe than the

cathodic evolution of H_2. Moreover, the E_{corr} values in presence of BPSs reveal a small change compared to that of the blank solution. Therefore, the inhibitor was defined as mixed type [22–24].

The values of corrosion potential (E_{corr}), cathodic Tafel slope (β_c), anodic Tafel slope (β_a), corrosion current density (i_{corr}), and the inhibition efficiency (η) are given in Table 3. Notably, the current density (i_{corr}), and the cathodic and anodic Tafel slopes were calculated by the Tafel extrapolation methods. Table 3 clearly shows that the *i*corr values decrease significantly after adding BPSs, suggesting that rate of corrosion reaction decreased because of the formation of a protective film of inhibitor on steel surface and this protective film created a barrier between the metal and corrosive medium.

Table 3. Polarization curve parameters of mild steel in 1 mol·L^{-1} HCl with various concentrations of BPSs at different temperatures

Inhibitors	C (mol·L^{-1})	$-E_{corr}$ (mV)	$-\beta_c$ (mV·dec^{-1})	i_{corr} (μA·cm^{-2})	η (%)
Blank	0	0.449	178	132	
4-BP	1×10^{-5}	0.451	172	141	90.4
	1×10^{-4}	0.440	163	122	93.9
	1×10^{-3}	0.448	165	143	97.6
	1×10^{-2}	0.432	171	155	98.7
2-BP	1×10^{-5}	0.436	174	142	88.7
	1×10^{-4}	0.442	167	125	92.9
	1×10^{-3}	0.453	162	132	96.3
	1×10^{-2}	0.469	163	128	97.7

In the meantime, η (%) increases with increasing inhibitor concentration. At 1×10^{-2} mol/L^{-1} for the inhibitors, the inhibition efficiency was 98.7% and 97.7% with 4-BP and 2-BP inhibitors, respectively. The inhibition properties of the inhibitors obtained from the polarization measurements also corresponded to those observed by the impedance data.

3.5 Adsorption isotherm study

The adsorption of an organic adsorbate on the surface of metal is regarded as a substitutional adsorption processes between the organic compound in aqueous phase and the water molecule adsorbed on the electrode surface. The Langmuir adsorption isotherm was found to be the best description of the adsorption behavior of the studied inhibitor, obeying the following equation [25].

$$\frac{\theta}{1-\theta} = K_{ads}C \qquad (6)$$

where C is the inhibitor concentration, θ is the fraction of the surface coverage (obtained from weight loss data), and K_{ads} is the adsorption constant.

Fig. 6 shows the straight line plot of log(θ/1-θ) *versus* log C. The strong correlation suggests that the adsorption of inhibitor on the metal surface obeyed the Langmuir's adsorption isotherm.

The high value of the adsorption constant reflects the high adsorption ability of this inhibitor on mild steel surface [26]; however, the K_{ads} values decreased with increasing temperature, indicating that the high temperature hampered the adsorption of the inhibitor and the inhibition process becomes less favorable with increasing temperature. The free energy (ΔG^0_{ads}) of the adsorption of the inhibitor on mild steel surface was evaluated by the following equation [27]:

$$K_{ads} = \frac{1}{C_{H_2O}} \exp\left(\frac{-\Delta G^0_{ads}}{RT}\right) \quad (7)$$

Generally, the values of ΔG^0_{ads} approximately –20 kJ·mol^{-1} or higher are consistent with physisorption, while those around –40 kJ·mol^{-1} or lower involve chemisorptions [28]. Table 4 shows the negative ΔG^0_{ads} values of the BPSs, indicating that the adsorption process takes place spontaneously. The absolute values of ΔG^0_{ads} calculated at different temperatures in the presence of BPSs ranged from 31 to 33 kJ·mol^{-1}, suggesting that BPSs adsorbed on the metal surface physically and chemically.

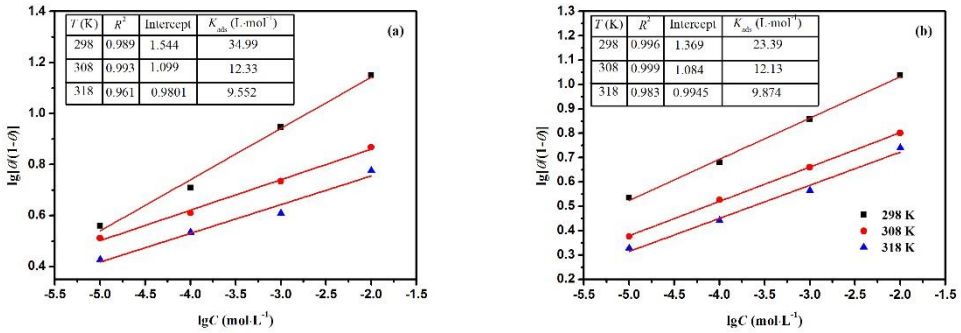

Figure 6. Adsorption isotherm for 4-BP (a) and 2-BP (b) on the surface of mild steel in 1 mol·L^{-1} HCl at different temperatures

Activation energy was calculated using the following relationship:

$$\ln r = -\frac{E_a}{RT} + \ln A \quad (8)$$

where r is the corrosion rates. The activation energies obtained by the plots of ln$r$ *versus* 1/T (Figure 7), the activation energy can be calculated by the slope, which are given in Table 5. E_a increases with increasing inhibitor concentration, indicating strong adsorption of inhibitor molecules at the metal surface. During the corrosion reaction mechanism the charge transfer is blocked with adsorption of BPSs to the metal surface, increasing the activation energy [29–32].

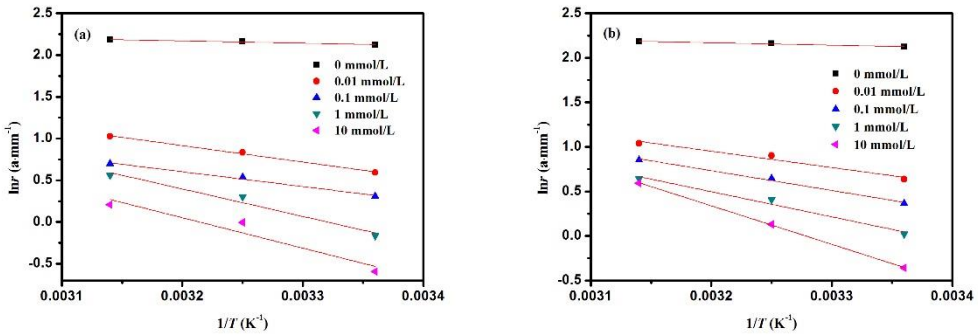

Figure 7. lnr versus 1/T plots of 4-BP (a) and 2-BP (b)

The enthalpy of adsorption (ΔH) is calculated from the equation [33].

$$\Delta H = E_a - RT \quad (9)$$

The thermodynamic parameters and the entropy (ΔS) of the BPSs have been calculated from the relationship:

$$\Delta G = \Delta H - T\Delta S \quad (10)$$

The calculated values of ΔH and ΔS over the temperature range 298–318K are also listed in Table 4. The positive value of ΔH reflects the endothermic nature of mild steel dissolution process, suggesting slow dissolution of mild steel [34]. The positive value of ΔS is attributed to the increase in disorder due to the adsorption of only one inhibitor molecule by desorption of more water molecules [35].

Table 4. The thermodynamic parameters for the corrosion of mild steel in the presence of BPSs

Inhibitors	T (K)	ΔH (kJ·mol^{-1})	ΔS (J·mol^{-1}·K^{-1})	ΔG (kJ·mol^{-1})
4-BP	298	21	178	-32
	308	20	171	-32
	318	20	167	-33
2-BP	298	22	180	-32
	308	22	174	-32
	318	22	170	-33

Table 5. Activation energy for corrosion of mild steel in the presence of BPSs

C (mol·L^{-1})	4-BP		2-BP	
	slope	Ea (kJ·mol^{-1})	slope	Ea (kJ·mol^{-1})
0	-287.5	2.391	-287.5	2.391
1×10^{-5}	-2052	17.06	-1919	15.95
1×10^{-4}	-1854	15.41	-2324	19.32
1×10^{-3}	-3442	28.62	-2954	24.56
1×10^{-2}	-3814	31.71	-4508	37.48

3.6 Surface analysis

The SEM images of the corroded surfaces for steel substrates in 1 mol·L^{-1} HCl solution with and without inhibitor after 3 h are shown in Fig. 8. The SEM image presented in Fig. 8(b) shows the severely deteriorated action of corrosive medium where the mild steel surface becomes damaged, porous, and highly rough covered with a thick porous oxide layer because of severe corrosion. Moreover, a steel sample treated with BPSs shows a minimum surface degradation, and the striations produced during polishing are thoroughly covered by a film of the inhibitor. A similar observation was reported [36,37]. Thus, BPSs have an ability to strongly adhere on the top of mild steel surface and protect steel from further corrosion against corrosion medium.

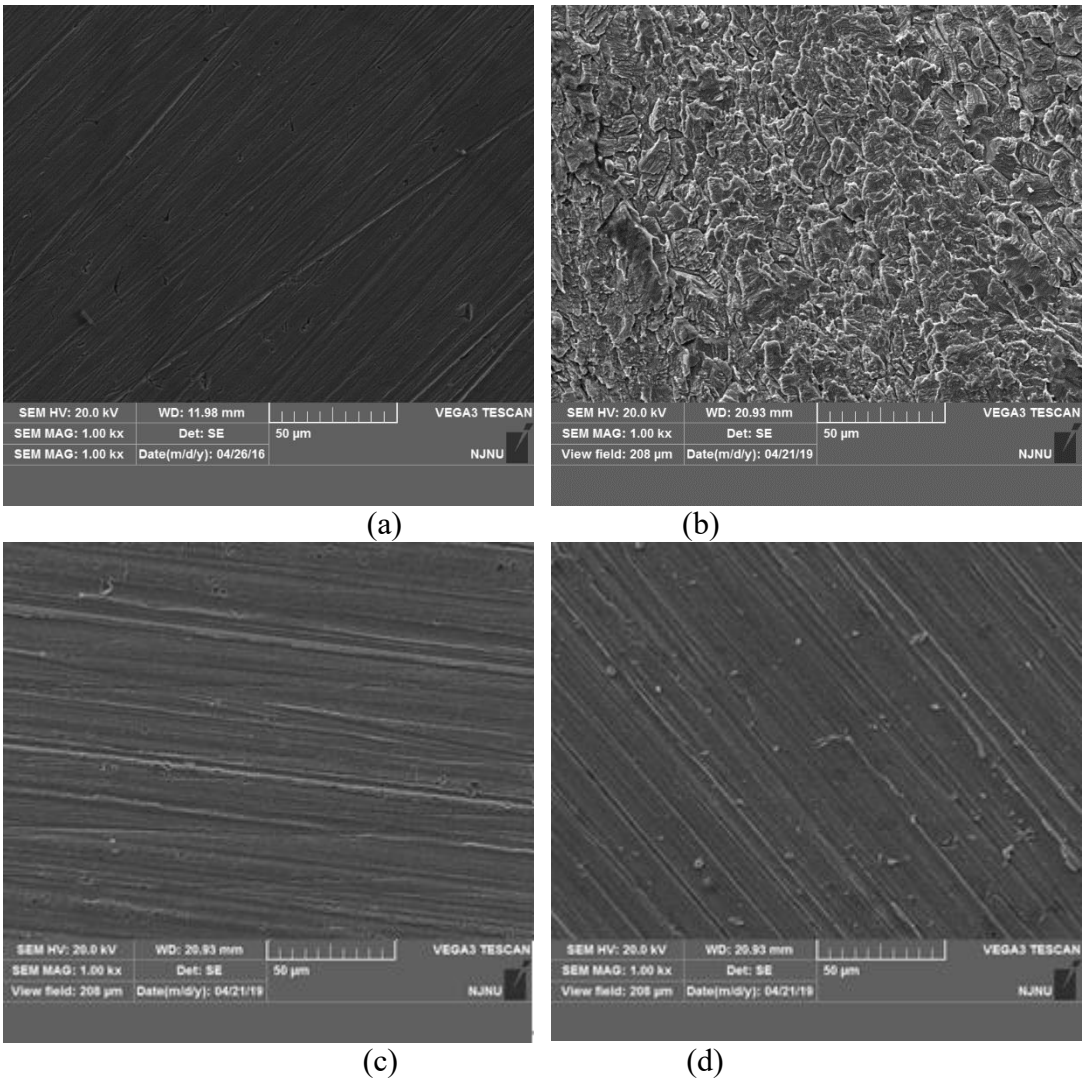

Figure 8. SEM images recorded after polished (a) and immersion of samples in 1 mol·L^{-1} HCl solution in the absence (b) or in the presence of 4-BP (c) and 2-BP (d)

The atomic force microscopy images of the samples are shown in Fig. 9, indicating that the blank sample shows highly rough surface due to corrosion, whereas the morphology in the presence of 1×10^{-2}

mol/L BPSs is strikingly different. The average roughness of the blank sample surface is 29.1 nm. The reduction in the average roughness to 4.59 nm and 19.5 nm on mild steel surface exposed to acid solution in the presence of 1×10^{-2} mol/L of BPSs confirms that the presence of inhibitor protects mild steel from corrosive solution [38–40].

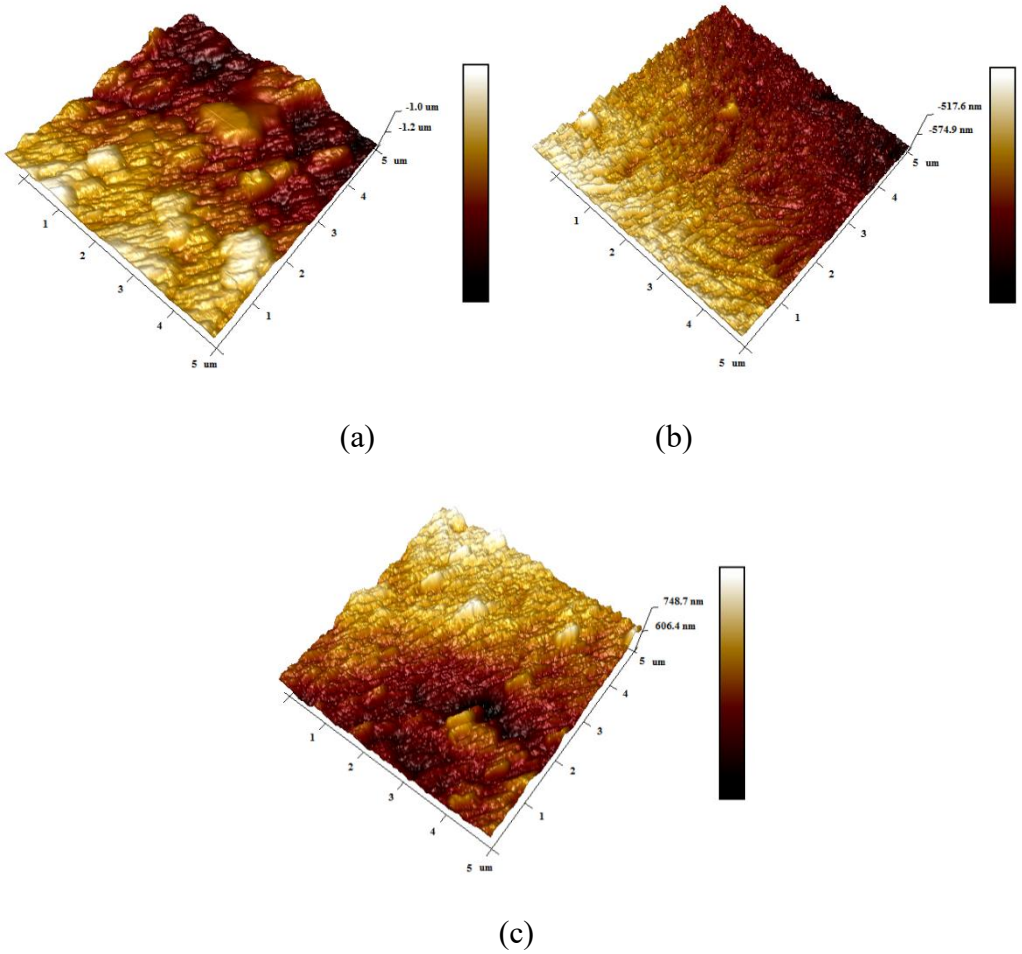

Figure 9. AFM images recorded after immersing in 1 mol·L^{-1} HCl solution in the absence (a) or in the presence of 4-BP (b) and 2-BP (c)

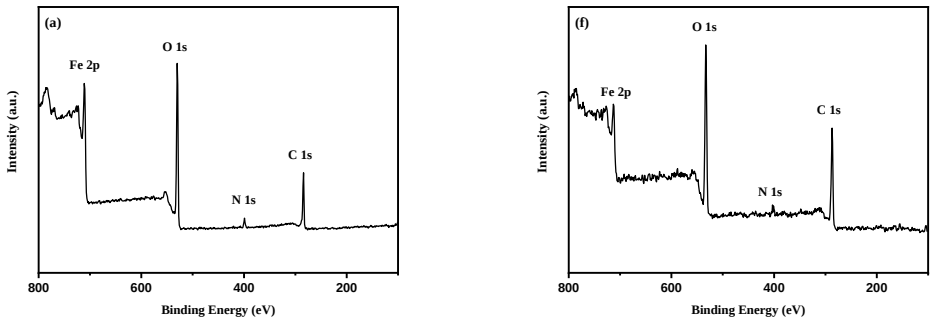

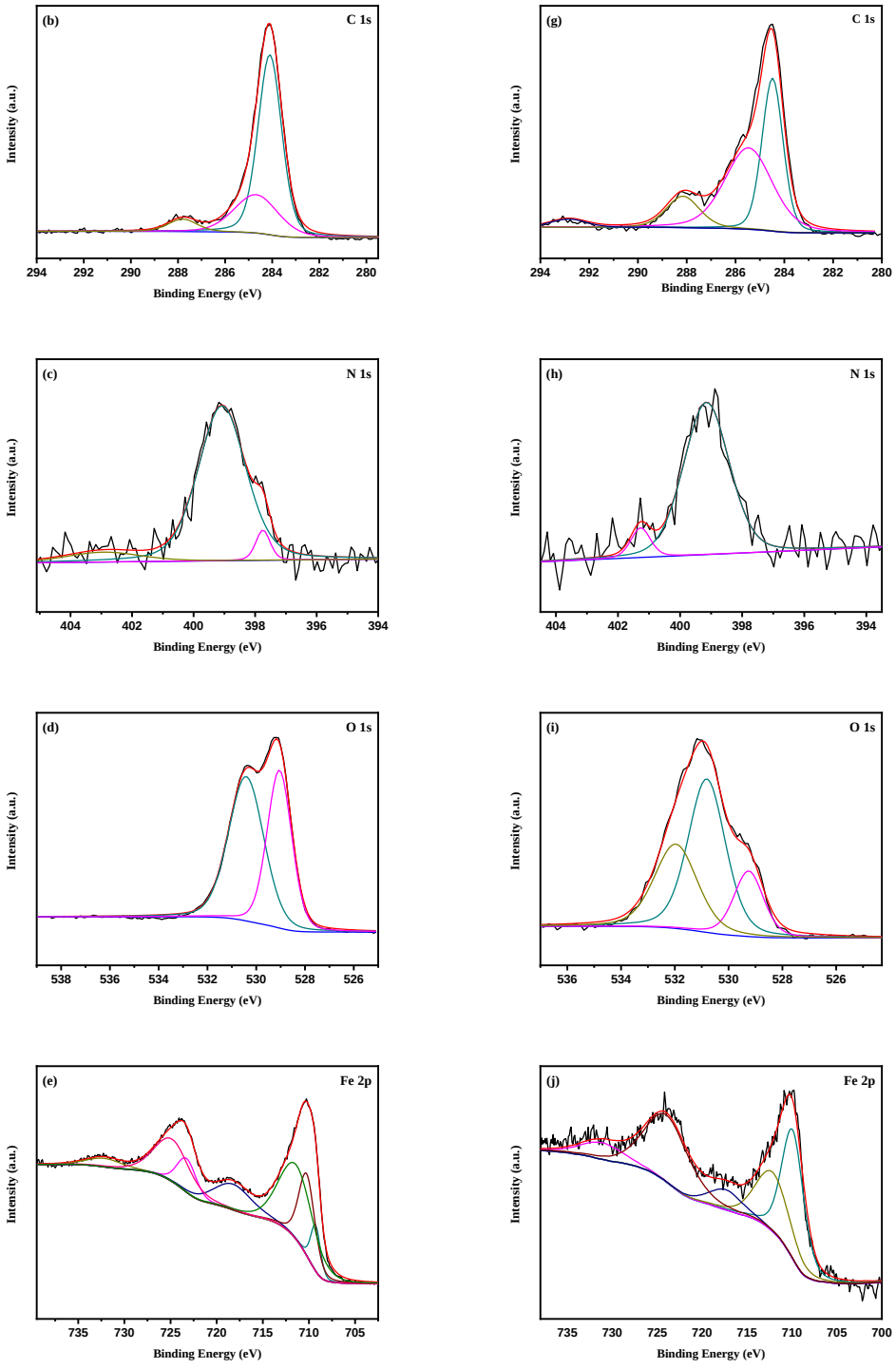

Figure 10. XPS analysis of BPSs: 4-BP (a)~(e) and 2-BP (f)~(j)

XPS technique was used to investigate the composition of the organic adsorbed layer on the mild steel surface in normal hydrochloric medium by BPSs. The results showed that the surface film generally comprises ferric oxide and carbonaceous organics. In this way, the high-resolution peaks for C 1s, O 1s, N 1s, and Fe 2p for mild steel surface after 3 h of immersion in 1M HCl solution containing 1×10^{-2} mol/L of BPSs are recorded, as shown in Fig. 10.

The C 1s spectra of 4-BP and 2-BP show three peaks (287.8, 284.7, and 284.1) and (288.2, 285.5, and 284.2), respectively. The largest peak can be attributed to the C–C and C=C aromatic bonds with the characteristic binding energy of 284.1 eV, whereas the peak at 284.2 eV in 2-BP as well. The peaks at 284.7 or 285.5 eV referred to the C–H, and those at 287.8 or 288.2 eV referred to the C–N and C=N, respectively [41–43]. The O 1s spectrum envelops were fitted by two peaks. The first peak located at 529.0 eV was attributed to Fe_2O_3 and/or Fe_3O_4 oxides [44]. The second peak located at 530.5 eV (530.8 eV for 2-BP) is attributed to the oxygen in hydrous iron oxides, such as FeOOH and/or $Fe(OH)_3$ [44]. The peaks of the N 1s of the steel sample treated by 4-BP may be fitted into three peaks located at 402.9, 399.1, 397.8 eV corresponding to the quaternary nitrogen ($=N^+$-) atom of the quinolinium ring [45], coordinated nitrogen atom, and C-N-metal bond [46,47], respectively. In case of 2-BP, these peaks are observed at 401.3 and 399.2 eV.

The Fe 2p spectra were fitted to two doublets, 711.7 eV or 712.7 (Fe 2p3/2) and 724.3 eV or 724.6 (Fe 2p1/2), with an associated ghost structure. The peak is attributable to the Fe–N, which is reported to appear at 710.3 eV (711.7 eV for 2-BP) [48,49]. The peak located at 711.7 or 712.7 eV was assigned to ferric compounds such as FeOOH (i.e., oxyhydroxide), Fe_2O_3 (i.e., Fe^{3+} oxide), and/or Fe_3O_4 (i.e., Fe^{2+}/Fe^{3+} mixed oxide) [50,51]; the peak observed at 718.6 or 718.7 eV may be ascribed to the satellite of Fe(III) [48]. Based on the previous observations, the XPS results support the presence of adsorbed BPSs on the carbon steel surface.

4. CONCLUSION

The conclusions of using 4-BP and 2-BP as the inhibitors of mild steel are as follows.

(1) The weight loss test and electrochemical results show that the anticorrosion efficiencies of BPSs increase with increasing inhibitor concentration, decrease with increasing temperature. In addition, BPSs act as a mixed-type corrosion inhibitor.

(2) The adsorption of BPSs can be described by the Langmuir adsorption isotherm, and the calculated free energy indicated chemisorption and physisorption nature of the absorption of the inhibitors on the steel surface.

(3) The surface analyses indicated that the inhibitor molecules adsorbed on the surface of mild steel to form a protective film, preventing corrosion resulting from the corrosive medium.

ACKNOWLEDGEMENTS

The authors gratefully acknowledges the support of the Open Fund of Shandong Key Laboratory of Corrosion Science (KLCS201901); and the Opening Project of Material Corrosion and Protection Key Laboratory of Sichuan province (2019CL14).

References

1. M. Allaoui, O. Rahim, L. Sekhri, *Orient. J. Chem.,* 33 (2017) 637.
2. H. Ashassi-Sorkhabi, D. Seifzadeh, M. Hosseini, *Corros. Sci.,* 50 (2008) 3363.

3. M. Elayyachy, A.E. Idrissi, B. Hammouti, *Corros. Sci.,* 48 (2006) 2470.
4. K.C. Emregul, M. Hayvali, *Corros. Sci.,* 48 (2006) 797.
5. M. Quraishi, D. Jamal, *J. Appl. Electrochem.*, 32 (2002) 425.
6. E.A. Noor, *Corros. Sci.,* 47 (2005) 33.
7. A. Popova, M. Christov, *Corros. Sci.,* 48 (2006) 3208.
8. J. Talati, D. Gandhi, *Corros. Sci.,* 23 (1983) 1315.
9. J. Halambek, K. Berkovic, J. Vorkapic-Furac, *Corros. Sci.*, 52 (2010) 3978.
10. P.C. Okafor, E.E. Ebenso, A.Y. El-Etre, M.A. Quraishi, *Int. J. Corros.,* 2012 (2012) 1.
11. A.M. Abdel-Gaber, B.A. Abd-El-Nabey, I.M. Sidahmed, A.M. El-Zayady, M. Saadawy, *Corros. Sci.*, 48 (2006) 2765.
12. E.E. Oguzie, *Corros. Sci.*, 50 (2008) 2993.
13. T Espinosa, J Sanes, A E Jimenez, *Appl. Surf. Sci.,* 273 (2013) 578.
14. E. Kowsari, S. Y. Arman, M. H. Shahini, H. Zandi, M. Mehdipour. *Corros. Sci.,* 112 (2016) 73.
15. S. M. Tawfik, *J. Mol. Liq.,* 216 (2016) 624.
16. A. P. Hanza, R. Naderi, E. Kowsari, M. Sayebani, *Corros. Sci.*, 107 (2016) 96.
17. Y. Qiang, S. Zhang, L. Guo, X. Zheng, B. Xiang, S. Chen, *Corros. Sci.*, 119 (2017) 68.
18. E. Gutierrez, J.A. Rodríguez, J. Cruz-Borbolla, J.G. Alvarado-Rodriguez, P. Thangarasu, *Corros. Sci.*, 108 (2016) 23.
19. H. Tian, W. Li, B. Hou, *Corros. Sci.*, 53 (2011) 3435.
20. L. Hu, S. Zhang, W. Li, B. Hou, *Corros. Sci.*, 52 (2010) 2891.
21. B. Tan, S. Zhang, Y. Qiang, L. Feng, C. Liao, Y. Xu, S. Chen, *J. Mol. Liq.*, 248 (2017) 902.
22. Q. H. Wang, B. C. Tan, H. B. Bao, Y. T. Xie, *Bioelectrochem.,* 128 (2019) 49.
23. Y. Yan, W. Li, L. Cai, B. Hou, *Electrochim. Acta*, 53 (2008) 5953.
24. B. Tan, S. Zhang, Y. Qiang, L. Guo, L. Feng, C. Liao, Y. Xu, S. Chen, *J. Colloid Interface Sci.*, 526 (2018) 268.
25. Y. Qiang, S. Zhang, S. Xu, L. Yin, *RSC Adv.*, 5 (2015) 63866.
26. G. Sigircik, T. Tuken, M. Erbil, *Corros. Sci.*, 102 (2016) 437.
27. N. El Hamdani, R. Fdil, M. Tourabi, C. Jama, F. Bentiss, *Appl. Surf. Sci.*, 357 (2015) 1294.
28. Z. Hu, Y. Meng, X. Ma, H. Zhu, J. Li, C. Li, D. Cao, *Corros. Sci.*, 112 (2016) 563.
29. Z. O. R. Sibel, D. Pinar, Y. Birgul, *Corros. Rev.*, 23 (2005) 217.
30. M. M. Osman, R. A. El-Ghazawy, A. M. Al-Sabagh, *Mater. Chem. Phys.* 80 (2003) 55.
31. D. Gopi, N. Bhuvaneswaran, S. Rajeswarai, K. Ramadan, *Anti-Corros. Methods Mater.*, 47 (2000) 332.
32. M. A. Ameer, E. Khamis, G. Al-Senani, *J. Appl. Electrochem.,* 32 (2002) 149.
33. L. J. M. Vracar, D. M. Dragic, *Corros. Sci.*, 44 (2002) 1669.
34. G. N. Mu, X. M. Li, F. Li, *Mater. Chem. Phys.*, 86 (2004) 59.
35. M. M. Saleh, *Mater. Chem. Phys.*, 98 (2006) 83.
36. A. R. Torres, M. G. V. Cisneros, J. G. G. Rodrigueza, *Green Chem. Lett. Rev.*, 9 (2016) 143.
37. S. Varvara, R. Bostan, O. Bobis, L. Gaina, F. Popad, V. Menae, R. M. Soutoe, *Appl. Surf. Sci.*, 426 (2017) 1100.
38. C. Kamal, M. G. Sethuraman, *Mater. Corros.*, 64 (2013) 1.
39. S. Varvara, R. Bostan, O. Bobis, L. Gaina, F. Popad, V. Menae, R. M. Soutoe, *Appl. Surf. Sci.*, 426 (2017) 1100.
40. A. Dehghani, G. Bahlakeh, B. Ramezanzadeh, *Bioelectrochem.*, 130 (2019) 107339.
41. J. F. Watts, J. Wolstenholme, An Introduction to Surface Analysis by XPS and AES, John Wiley and Sons Inc., (2003) London, UK.
42. C. D. Wanger, W. M. Riggs, L. E. Davis, J. F. Moulder and G. E.Muilenberg, Handbook of X-Ray Photoelectron Spectroscopy, Perking-Elmer Corporation, Physical Electronics Divisionm, (1979) Minnesota, USA.
43. T. Yamashita, P. Hayes, *Appl. Surf. Sci.,* 254 (2008) 2441.

44. W. Temesghen, P. M. A. Sherwood, *Anal. Bional. Chem.,* 373 (2002) 601.
45. Y. Tang, F. Zhang, S. Hu, Z. Cao, Z. Wu, W. Jing, *Corros. Sci.,* 74 (2013) 271.
46. L. T. Weng, C. Poleunis, P. Bertrand, V. Carlier, M. Sclavons, P. Franquinet, R. Legras, *J. Adhes. Sci. Technol.,* 9 (1995) 859.
47. M. Finsgar, S. Fassbender, S. Hirth, I. Milosev, *Mater. Chem. Phys.*, 116 (2009) 198.
48. S. Ciampi, V. Di castro, *Surf. Sci.*, 331 (1995) 294.
49. S. D. Zhang, J. Wu, W. B. Qi, J. Q. Wang. *Corros. Sci.*, 110 (2016) 57.
50. M. A. Pech-Canul, P. Bartolo-Perez, *Surf. Coat. Technol.*, 184 (2004) 133.
51. F. Z. Bouanis, F. Bentiss, M. Traisnel, C. Jama. *Electrochim. Acta*, 54 (2009) 2371.